Exp Astron (2012) 34:551–582
DOI 10.1007/s10686-011-9255-0

ORIGINAL ARTICLE

GRIPS - Gamma-Ray Imaging, Polarimetry and Spectroscopy

Jochen Greiner · Karl Mannheim · Felix Aharonian · Marco Ajello · Lajos G. Balasz · Guido Barbiellini · Ronaldo Bellazzini · Shawn Bishop · Gennady S. Bisnovatij-Kogan · Steven Boggs · Andrej Bykov · Guido DiCocco · Roland Diehl · Dominik Elsässer · Suzanne Foley · Claes Fransson · Neil Gehrels · Lorraine Hanlon · Dieter Hartmann · Wim Hermsen · Wolfgang Hillebrandt · Rene Hudec · Anatoli Iyudin · Jordi Jose · Matthias Kadler · Gottfried Kanbach · Wlodek Klamra · Jürgen Kiener · Sylvio Klose · Ingo Kreykenbohm · Lucien M. Kuiper · Nikos Kylafis · Claudio Labanti · Karlheinz Langanke · Norbert Langer · Stefan Larsson · Bruno Leibundgut · Uwe Laux · Francesco Longo · Kei'ichi Maeda · Radoslaw Marcinkowski · Martino Marisaldi · Brian McBreen · Sheila McBreen · Attila Meszaros · Ken'ichi Nomoto · Mark Pearce · Asaf Peer · Elena Pian · Nikolas Prantzos · Georg Raffelt · Olaf Reimer · Wolfgang Rhode · Felix Ryde · Christian Schmidt · Joe Silk · Boris M. Shustov · Andrew Strong · Nial Tanvir · Friedrich-Karl Thielemann · Omar Tibolla · David Tierney · Joachim Trümper · Dmitry A. Varshalovich · Jörn Wilms · Grzegorz Wrochna · Andrzej Zdziarski · Andreas Zoglauer

Received: 4 May 2011 / Accepted: 9 August 2011 / Published online: 26 August 2011

Abstract We propose to perform a continuously scanning all-sky survey from 200 keV to 80 MeV achieving a sensitivity which is better by a factor of 40 or more compared to the previous missions in this energy range (COMPTEL, INTEGRAL; see Fig. 1). These gamma-ray observations will be complemented by observations in the soft X-ray and (near-)infrared region with the corresponding telescopes placed on a separate satellite. The Gamma-Ray Imaging, Polarimetry and Spectroscopy ("**GRIPS**") mission with its

See Web-site www.grips-mission.eu for the authors' affiliations.

J. Greiner (✉)
MPI für extraterrestrische Physik, 85740 Garching, Germany
e-mail: jcg@mpe.mpg.de

K. Mannheim
Inst. f. Theor. Physik & Astrophysik, Univ. Würzburg, 97074 Würzburg, Germany
e-mail: mannheim@astro.uni-wuerzburg.de

three instruments Gamma-Ray Monitor (GRM), X-Ray Monitor (XRM) and InfraRed Telescope (IRT) addresses fundamental questions in ESA's Cosmic Vision plan. Among the major themes of the strategic plan, GRIPS has its focus on the evolving, violent Universe, exploring a unique energy window. We propose to investigate γ-ray bursts and blazars, the mechanisms behind supernova explosions, nucleosynthesis and spallation, the enigmatic origin of positrons in our Galaxy, and the nature of radiation processes and particle acceleration in extreme cosmic sources including pulsars and magnetars. The natural energy scale for these non-thermal processes is of the order of MeV. Although they can be partially and indirectly studied using other methods, only the proposed GRIPS measurements will provide direct access to their primary photons. GRIPS will be a driver for the study of transient sources in the era of neutrino and gravitational wave observatories such as IceCUBE and LISA, establishing a new type of diagnostics in relativistic and nuclear astrophysics. This will support extrapolations to investigate star formation, galaxy evolution, and black hole formation at high redshifts.

Keywords Compton and Pair creation telescope · Gamma-ray bursts · Nucleosynthesis · Early Universe

1 Introduction

Photon energies between hard X-rays of 0.2 MeV and γ-rays of 80 MeV cover the range where many of the most-spectacular cosmic sources have their peak emissivity, so that essential physical processes of high-energy astrophysics can be studied most directly. Moreover, excitation and binding energies of atomic nuclei fall in this regime, which therefore is as important for high-energy astronomy as optical astronomy is for phenomena related to atomic physics. In addition, it includes the energy scale of the electron and pion rest mass. Current instrument sensitivities expose an "MeV-gap" exactly over this range (Fig. 1, left). The GRIPS mission with its prime instrument GRM (Gamma-Ray Monitor) will improve the sensitivity in this gap by a factor of 40 compared to previous missions. Therefore, the GRIPS all-sky survey with γ-ray imaging, polarimetry, and spectroscopy promises new discoveries, beyond its precision diagnostics of primary high-energy processes. In addition, the auxiliary instruments XRM (X-ray monitor) and IRT (InfraRed Telescope; see Section 3 for details) will provide broad-band coverage, thus helping in identification of counterparts and emission processes.

GRIPS would open the astronomical window to the bizarre and highly variable high-energy sky, to investigate fascinating cosmic objects such as γ-ray bursts, blazars, supernovae and their remnants, accreting binaries with white dwarfs, neutron stars or black holes often including relativistic jets, pulsars and magnetars, and the often peculiar cosmic gas in their surroundings. Many of these objects show MeV-peaked spectral energy distributions (Fig. 1, right) or

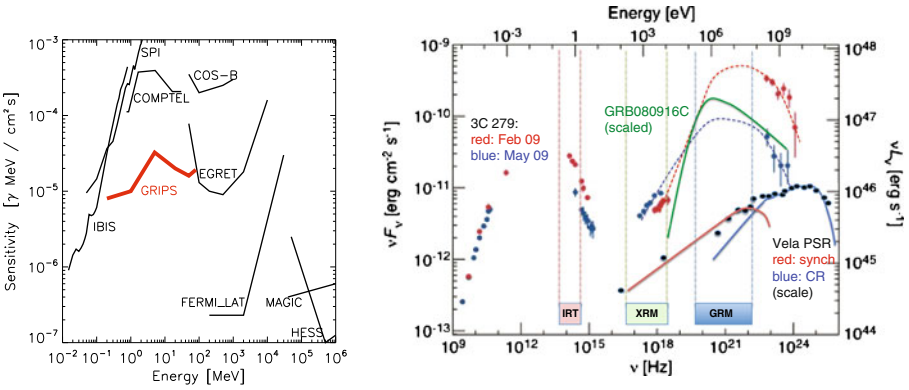

Fig. 1 *Left* GRIPS would contain three instruments: GRM, XRM and IRT. The Gamma-Ray monitor (GRM) will allow a major sensitivity improvement in an energy range (between hard X-rays and GeV γ-rays) which has been poorly explored, yet holds unique information for a wide range of astrophysical questions. The curves are for an exposure of 10^6 s, $\Delta E = E$, and an E^{-2} spectrum. *Right* Not only GRBs, but also blazar SEDs peak in the MeV range, and pulsars turn over from their maximum in the *Fermi* band. The combined γ-, X-ray and near-infrared coverage of blazars by the three GRIPS instruments covers both emission components simultaneously

characteristic spectral lines; we target such primary emission to understand the astrophysics of these sources.

Unrivaled by any other method, the detection of highly penetrating γ-rays from cosmological γ-ray bursts will shed light on the first massive stars and galaxies which formed in obscuring gas clouds during the dark ages of the early Universe. Polarization measurements of γ-ray bursts and blazars will for the first time decipher the mechanism of jet formation in accreting high-spin black hole systems ranging from stellar to galactic masses.

The primary energy source of supernova (SN) light is radioactive decay, deeply embedded below the photosphere as it appears in conventional astronomical bands. The first direct measurement of the nickel and cobalt decay inside Type Ia SNe will pin down their explosion physics and disentangle their progenitor channels. This will impact the luminosity calibration of Type Ia SNe that serve as standard candles in cosmology. Similarly, the otherwise unobtainable direct measurement of the inner ejecta and the explosive nucleosynthesis of core collapse supernovae will allow to establish a physical model for these important terminal stages of massive-star evolution. Explosion asymmetries [21] and the links to long GRBs are important aspects herein. Pair-instability supernovae from very massive stars will be unambiguously identified through their copious radioactivity emission. These observations will be crucial for complementing neutrino and gravitational wave measurements, and for our understanding of the astrophysical processes and sources which underly and generate cosmic chemical evolution.

Nuclear de-excitation lines of abundant isotopes like ^{12}C and ^{16}O, the hadronic fingerprints of cosmic-ray acceleration, are expected to be discovered

with GRIPS [42]. Understanding the relative importance of leptonic and hadronic processes, and the role of cosmic rays in heating and ionizing molecular clouds and thus seeding interstellar chemistry will boost our understanding of both relativistic-particle acceleration and the cycle of matter. The detection of instabilities in the supercritical magnetospheres of magnetars, which are expected to lead to few-hundred keV to possibly MeV-peaked emission, will explore white territory on the field of plasma physics. Resolving the riddle of the positron annihilation line will shed new light on dark matter annihilation and other sources of anti-matter in the Galaxy.

We detail in the following sub-sections how GRIPS will answer the burning questions: *How do stars explode? What is the structure of massive-star interiors and of compact stars? How are cosmic isotopes created and distributed? How does cosmic-ray acceleration work? How is accretion linked with jets?* Answering these questions will provide the basis to understand the larger astrophysical scales, like the interstellar medium as it evolves in galaxies, the supernova-fed intergalactic gas in galaxy clusters, and the cosmic evolution of elemental abundances.

The version of GRIPS described here is the result of further development and improvement of the original design concept as proposed for CV2007 [19]. The major improvements/differences can be summarized as follows: (1) improved sensitivity at low energies, (2) extended energy range up to 80 MeV, (3) less power consumption due to smaller number of channels, (4) inclusion of an InfraRed Telescope (IRT) in addition to GRM and XRM, (5) a different flight configuration, and (6) broader science coverage.

2 Scientific objectives

2.1 Gamma-ray bursts and first stars

GRIPS will observe in the energy range where GRB emission peaks. With its energy coverage up to 80 MeV, GRIPS will firmly establish the high energy component seen in *CGRO*/EGRET (>10 MeV) and *Fermi*/LAT bursts (>100 MeV) in much larger numbers, and characterize its origin through polarisation signatures. GRIPS will measure the degree of polarisation of the prompt γ-ray burst emission to a few percent accuracy for more than 10% of the detected GRBs (see simulations in Section 4), and securely measure how the degree of polarisation varies with energy and/or time over the full burst duration for dozens of bright GRBs. Also, the delay of GeV photons relative to emission at $\sim$ hundred keV, observed in a few GRBs with *Fermi*/LAT, manifests itself already at MeV energies in *Fermi*/GBM, and will thus be a science target for GRIPS. These observations enable a clear identification of the prompt GRB emission processes, and determine the role played by magnetic fields.

Due to its outstanding sensitivity (Fig. 2), GRIPS will detect $\sim$ 650 GRBs yr^{-1}, among those 440 GRBs yr^{-1} with good positions and XRM follow-

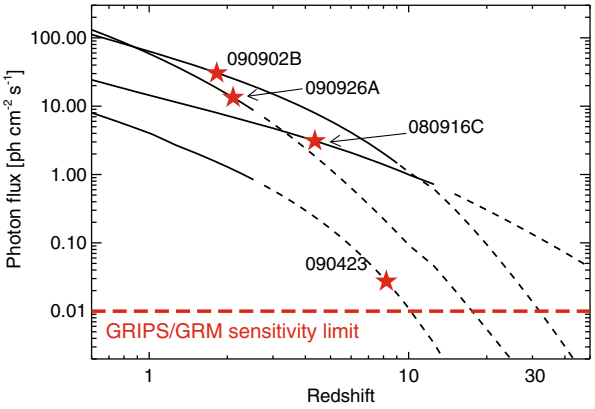

Fig. 2 The 0.2–2 MeV GRB peak photon flux as a function of burst redshift. The positions of three *Fermi*/GBM+LAT GRBs as well as the highest redshift GRB 090423 [40, 43] are indicated (stars) with their predicted peak fluxes. The crossing of the dashed curves with the sensitivity curve (horizontal red line; 1 s, 30° off-axis) marks the largest redshift up to which these bursts would be detectable with GRIPS. The transition between solid and dashed curves marks the redshift below which also $E_{\rm peak}$ can be measured with GRIPS

up, and measure the incidence of gas and metals through X-ray absorption spectroscopy and line-of-sight properties by enabling NIR spectroscopy with *JWST*. GRIPS should detect more than 20 GRBs at $z > 10$ over 10 years, and the IRT will determine photometric redshifts for the bulk of the $z > 7$ sources (Fig. 3). With the detection of at least one $z > 20$ event during the mission lifetime, the high-z detection rate is high enough to clearly detect the cut-off

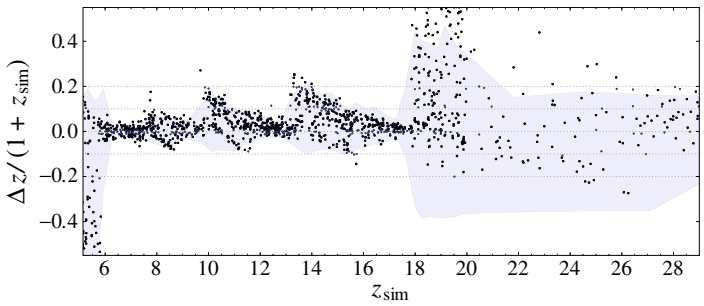

Fig. 3 GRB afterglow photometric redshift accuracy of the IRT filter set as in 17. *Black dots* show 900 simulated afterglows and *shaded area* represents the 1σ statistical uncertainty of the photo-z analysis averaged over 30 afterglows in relative ($\eta = \Delta z/(1+z)$) terms. For the $7 < z < 17$ redshift range, the photo-z can be determined to better than 20%. The apparent steps (increase of η) at $z \approx 8$, 10, 13, 18 happen when Ly-α falls between two filters, e.g. Y and J for $z \approx 8$; these steps increase as the gaps between the filters are larger at longer wavelength. At $z > 17.5$ (K-dropout), the error gets larger due to the gap above the K band and the widths of the L (M) bands; yet, the redshift accuracy is more than sufficient for any follow-up decision

in the z-distribution IF star formation starts at a certain redshift (below ∼35) throughout the Universe, as theory suggests [11, 32]. Measuring this cut-off, or no cut-off up to $z \sim 25$, would in turn be a limit to the earliest time when stars formed.

If the GRB environments contain total hydrogen column densities of 10^{25} cm^{-2}, or higher, GRIPS holds the promise of measuring redshifts directly from the γ-ray spectrum via nuclear resonances [23] (Fig. 4), and will be sensitive to do so beyond z∼13.

GRIPS will also detect a handful of short GRBs at very low redshift ($z < 0.1$) during its mission lifetime, enabling a potential discovery of correlated gravitational-wave and/or neutrino signals.

2.2 Blazars

The extragalactic sky at high-energies is populated with thousands of highly variable blazars and radio galaxies, most recently pictured with *Fermi* [2]. GRIPS will catalogue about 2,000 blazars, thus probing blazar evolution to large redshifts. These observations will pinpoint the most massive halos at large redshifts, thus severely constraining models of structure evolution. This large sample of blazars will establish their (evolving) luminosity function and thus determine the fractional contribution of blazars to the diffuse extragalactic background. GRIPS is expected to detect ∼10 blazars at z > 8.

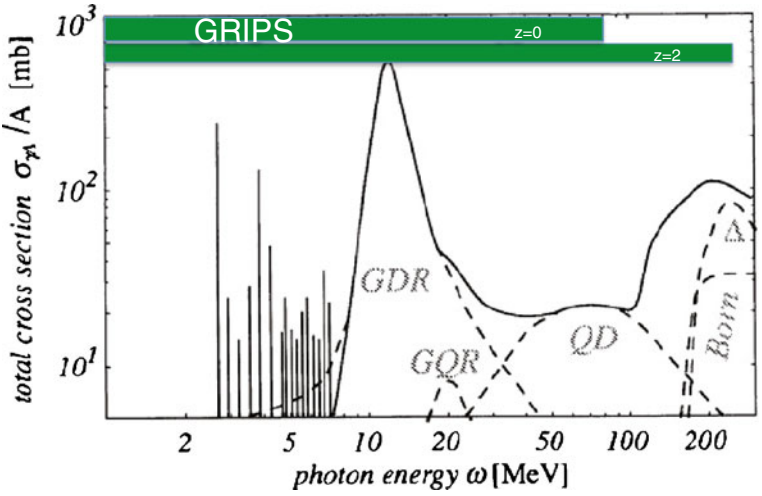

Fig. 4 Nuclear interactions with photons occur in the range of nuclear excitation levels (∼MeV), collective-nucleon resonances such as Pygmy (vertical lines; 3–10 MeV) and Giant Dipole resonances (GDR; 15–30 MeV), and individual nucleon excitations at higher energies such as the Delta resonance (Δ). GRIPS energies cover these line features, and thus provide a capability for measurements of fully-ionized matter in extreme plasma, when atomic transitions are absent

GRIPS observations in the MeV band will be crucial to disentangling leptonic and hadronic emission mechanisms. In leptonic scenarios, the MeV peak arises from external Compton scattering while in hadronic scenarios this is understood as the pile-up of cascade emission; both show markedly-different variability behaviour [9]. Studies of their nonthermal radiation mechanism will be supported through spectro-polarimetric measurements. The link between the inner accretion disk and the jet can be probed with correlated variability from the thermal to the nonthermal regime, using GRIPS auxiliary instruments. This will localize the dominant region of high-energy emission.

Through nuclear lines detected in nearby AGNs, and through tracing variability, GRIPS will probe the injection of accelerated particles into the jet plasma.

2.3 Supernovae and nucleosynthesis

GRIPS will search the nearby Universe out to 20 Mpc for ^{56}Ni decay γ-ray lines from SNIa, with an expectation of 10–20 significant detections. Establishing ratios of various lines from the ^{56}Ni decay chain (see Fig. 5), and their variation with time, are key GRIPS objectives. Even if the lines are significantly Doppler-broadened, the 0.1–3 MeV continuum can be used to test different explosion scenarios (e.g. [41]). Combined with optical-IR data, one can determine/constrain unburnt WD material [31], and with annihilation lines from ^{56}Co and ^{48}V decay positrons, one has a sensitive probe (via e^+ propagation) of the magnetic field structure (combed vs. scrambled) in expanding SNIa remnants.

GRIPS will also detect several nearby core-collapse supernovae (ccSNe). As for SNIa and SN1987A, the signature of γ-ray escape from the ejecta reflects hydrodynamic large scale mixing during and after the explosion. Comparing γ-ray line ratio and shape characteristics of different classes of SNe offers a direct view of the central supernova engines, and can help to reveal their progenitors. This includes pair-instability SNe [29] linked to GRBs which will be relatively enriched in the GRIPS sample from a larger sampling volume due to their high ($\sim$3 $M_\odot$) ^{56}Ni mass [16]. Depending on how deeply the radioactive ^{56}Ni may be embedded, GRIPS would detect between 0.1 and 10 ccSNe per year, the total-mission sample including 1–3 of the exotic and bright events (estimates are based on galaxy counts, scaling our Galaxy's ccSN rate for Milky-Way like galaxies from the Local Group, and a typical ccSN ^{56}Ni mass of 0.1 $M_\odot$. For SN1987A only 0.3% of its radioactive ^{56}Ni had been seen in line gamma-rays, and GRIPS would see a SN1987A-like signal from 1 Mpc distance; SNIb/c with their smaller envelope masses would be much brighter and seen from larger distance, as would hypernovae and pair instability supernovae). Thus, GRIPS will probe the range of variations currently discussed for supernova events from massive stars.

The Galactic census of ccSNe and their associated ^{44}Ti emission, deepened by an order of magnitude in flux by GRIPS, will sample ccSNe that occurred

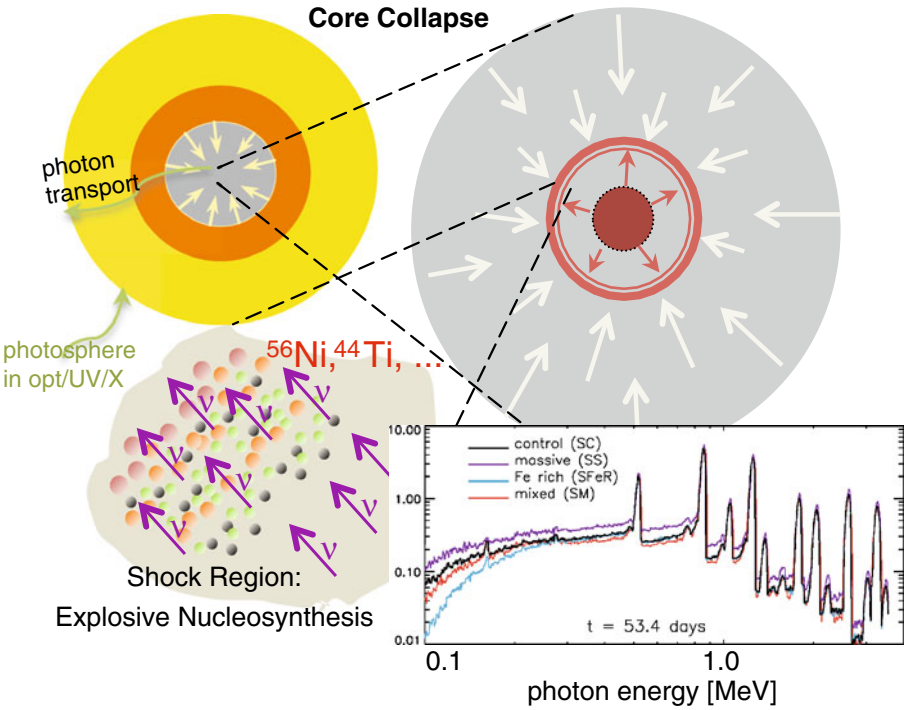

Fig. 5 Supernova light originates from ^{56}Ni radioactivity produced in their inner regions. Gamma-rays from radioactivity penetrate the SN envelope. Here a core-collapse SN is shown, with gamma-ray emitting isotopes such as ^{56}Ni being produced from infalling nuclei as these are decomposed and re-assembled. Gamma-ray lines and their changing relative intensities are direct messengers of the explosion physics, characteristic for the different SNIa and also core-collapse supernova variants

anywhere in the Galaxy during the past several centuries (estimated rate 1/50 yr). Presently, Cas A (age of 340 yr) is still the only clearly-detected ^{44}Ti source, while we expect to see about a handful of such young remnants. The (currently indirectly inferred) amount of ^{44}Ti in SN1987A will be measured with GRIPS at $>5\sigma$ significance. Since ^{44}Ti ejection is strongly linked to non-spherical explosions, the SN1987A measurement of ^{44}Ti together with the measurement of the subset of ^{44}Ti-emitting ccSNe will clarify the role of asphericities in ccSNe. Note the implications for GRBs, a SN class which is believed to be the extremes of core-collapses in terms of deviating from spherically-symmetric explosions.

Novae will be GRIPS-tested for ^{7}Be and ^{22}Na emission to distances of $\sim$5 kpc, resulting in valuable constraints for theoretical models. Predicted annihilation line flashes (from the decay of ^{18}F and ^{13}N) are detectable throughout the Galaxy, and since they occur prior to the optical emission, enable the

earliest possible detections of novae and early follow-up. The discovery of an unexpected high-energy emission in the symbiotic binary V407 Cygni, attributed to shock acceleration in the ejected nova shell after interaction with the wind of the red giant [3], opens up new possibilities that will be probed in more detail with GRIPS.

GRIPS will measure diffuse radioactivity afterglows of nuclear burning inside massive stars and supernova, at the Myr time scale (^{26}Al and ^{60}Fe decays), for dozens of nearby (∼kpc) stellar associations and groups. Combined with the stellar census for these groups as obtained from other observations (e.g. *GAIA*), this provides unique measurements of isotopic yields, serving as calibrators for nucleosynthesis in massive stars. These radioactivities also trace the flow and dynamical state of hot interstellar cavities, as they merge with the ambient ISM. Their radioactive clock directly relates to the age of the stellar group, and hence to the stellar-mass range that could have exploded as SN. For nearby ($\leq$ 1 kpc) stellar groups, the distribution of ejecta as compared to the parental molecular-cloud morphology thus provides a diagnostic for molecular-cloud destruction via feedback from massive stars and supernovae. GRIPS will provide a Galactic map of ^{60}Fe emission, essential for disentangling the contributions of different candidate source types to ^{26}Al. Line ratios for specific groups will constrain ^{60}Fe production of massive stars beyond ∼40 $M_\odot$, which directly relates to (uncertain) convective-layer evolution and stellar rotation [30] (Fig. 6). GRIPS will also detect these two key radioactivities, for the first time, in the local group (M31, LMC, SMC).

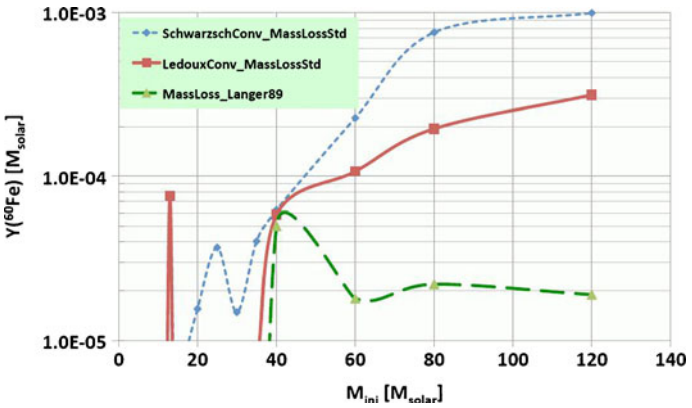

Fig. 6 Convection inside massive stars is complex, and the yields of ^{60}Fe are sensitive to detail. Variations with different prescriptions of convection zones (Ledoux versus Schwarzschild criterion), and mass loss (reduced versus Langer1989), affect ^{60}Fe yields for high-mass stars by up to an order of magnitude, respectively [30]

2.4 Annihilation of positrons

Recent observations of the 511 keV γ-ray line, accompanied by a lower-energy (∼100–511 keV) continuum with its own characteristic spectral shape, have produced results (Fig. 7) which are both surprising and challenging [36]. GRIPS will probe positron escape from candidate sources along the Galactic plane through annihilation γ-rays in their vicinity. For several microquasars and pulsars [36], point-source like appearance is expected if the local annihilation fraction $f_{\rm local}$ exceeds 10% ($I_\gamma \sim 10^{-2} \cdot f_{\rm local}$ ph cm^{-2} s^{-1}). GRIPS will enable the cross-correlation of annihilation γ-ray images with candidate source distributions, such as ^{26}Al and Galactic diffuse MeV emission (where it is dominated by cosmic-ray interactions with the ISM) [both also measured with GRIPS at superior quality], point sources derived from *INTEGRAL*, *Swift*, *Fermi*, and *H.E.S.S.* measurements of pulsars and accreting binaries, and with candidate dark-matter related emission profiles.

GRIPS will deepen the current *INTEGRAL* sky image by at least an order of magnitude in flux, at similar angular resolution. Comparing Galactic-disk and -bulge emission, limits on dark-matter produced annihilation emission will constrain decay channels from neutralino annihilation in the gravitational field of our Galaxy [14]. GRIPS will also be able to search for γ-ray signatures of dark matter for nearby dwarf galaxies [22].

2.5 Cosmic rays

Potential sources of cosmic rays can be observed through their γ-ray emission. At high energies, the ambiguity between inverse-Compton emission due to accelerated electrons and pion-decay γ-rays due to accelerated protons and ions cannot easily be resolved. GRIPS observations of diffuse nuclear de-excitation line spectra would therefore be of utmost diagnostic importance.

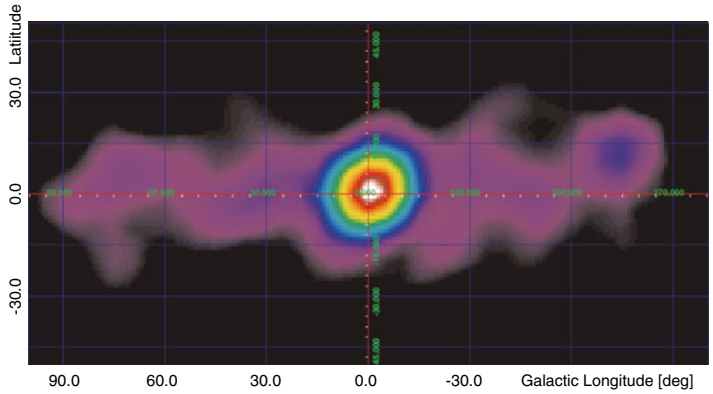

Fig. 7 *INTEGRAL/SPI* image of the annihilation emission at 511 keV along the inner Galaxy [10], illustrating the bright, dominating bulge-like emission. The color scales with S/N

Prime targets for the detection of these nuclear de-excitation lines in the 1–10 MeV energy band are the inner Galaxy and the Orion star-forming region [38]. Collisions of particles with energies above the thermal regime with interstellar gas are responsible for such excitation and emission, so that the acceleration process from the thermal pool to relativistic energies and the Cosmic-Ray-ISM connection will be probed with unprecedented sensitivity [44]. Furthermore, characteristic nuclear de-excitation lines expected from Wolf-Rayet enriched supernova remnant environments, could be discovered, testing one of the current CR origin models. Nuclear de-excitation lines produced in the environments of SNRs and accreting binaries offer unique laboratories for gauging models of cosmic ray production, acceleration, transport, and interaction with their surroundings. GRIPS will establish this tool for particle acceleration sites in the Galaxy, and will also contribute to this topic in the context of solar flares (see Section 2.7).

2.6 Compact stellar objects: pulsars, magnetars, accreting binaries

GRIPS will detect 30–40 pulsars in the 0.2–80 MeV energy range. This estimate is based on the pulsars in the Fermi catalogue [4] extrapolated to lower energies, as well as extrapolation to higher energies of the hard spectra of the youngest pulsars detected by *INTEGRAL* and *RXTE*/HEXTE at hard X-ray energies. Most of the latter pulsars appear to reach their maximum luminosity in the MeV regime. The left panel of Fig. 8 shows a few examples

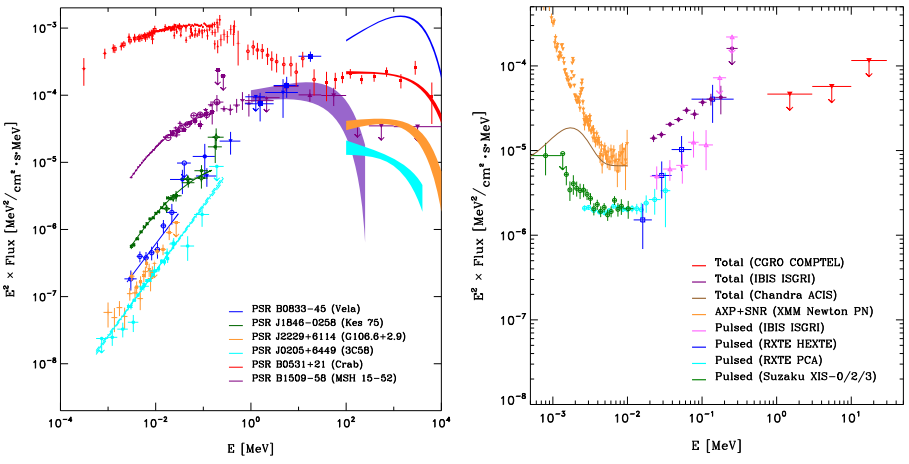

Fig. 8 *Left* Observed spectral energy distributions of a sample of young rotation-powered pulsars showing some examples of pulsars reaching their maximum luminosities in the MeV band. *Right* Observed spectral energy distribution of SNR Kes 73 and its compact object AXP 1E1841-045 (total and pulsed emissions). This illustrates the importance of sensitive measurements between 100 keV and 100 MeV to sample the break energy region

in comparison with the spectrum of the Vela pulsar, peaking in energy output at GeV energies, as most Fermi-detected pulsars do: The young PSR B1509-58 in MSH 15–52 reaches its maximum luminosity in the MeV band [1, 24, 35], as well as the young, radio weak pulsar PSR J0205+6449 [25]. The also young, radio quiet, high B-field PSR J1846-0258 has been detected at hard X-rays [26] with a similar spectral shape as PSR B1509-58, but not yet by Fermi/LAT, proving that its maximum luminosity is also reached in the MeV band. In fact, the figure shows that also the young Crab pulsar is peaking in energy output far below the GeV range.

Pulsar γ-radiation is produced by extremely relativistic ($\gamma \sim 10^6$–10^7) electrons (and positrons) propagating along the curved field lines close to the speed-of-light cylinder, which marks the outer extent of the co-rotating magnetosphere. Photon-electron cascades are generated by the interplay of electron curvature radiation, inverse Compton scattering (at GeV energies), synchrotron processes (MeV range) and pair creation from photon-B-field interactions. Since the particle flows are strongly aligned to the magnetic field, the emitted γ-rays delineate the field geometry and the relativistic plasma densities of their regions of origin. Furthermore one expects a significant imprint of polarisation in the emitted radiation, because the geometry is very anisotropic and the relevant emission processes are per se highly polarized from the predefined magnetic-field direction. GRIPS-determined light-curves and phase-resolved spectra in the 0.2–80 MeV range will provide decisive constraints on the HE-emission geometry in the pulsar magnetosphere and the acceleration processes located therein [6, 7, 39, 45]. For brighter pulsars, polarisation data will identify the nature of the emission.

Measurements of pulsar wind nebulae [15] (prominent examples at MeV energies are the Crab nebula and Vela X-1) will track the outflow of relativistic particles and fields.

'Magnetars' are neutron stars believed to have magnetic-field strengths of 10^{14}–10^{15} G, and manifest themselves as 'anomalous X-ray Pulsars' (AXPs) or 'soft gamma-ray repeaters' (SGRs). Pulsed radiation with a thermal spectrum at soft X-rays (1–10 keV) and an extremely hard power-law up to nearly 300 keV has been observed from 6–7 AXPs/SGRs [27]. GRIPS will search for photon splitting in strong B-fields in selected pulsars and AXPs/SGRs. Splitting suppresses the creation of pairs, and inhibits escape of any near-surface emission above about 10–20 MeV.

GRIPS will search for long orbit neutron star/massive star binaries and for tight accreting systems harboring neutron stars or black holes. These systems (e.g. Cyg X-1) exhibit hard power-law spectral tails beyond 100 keV when they are in their high/soft emission state. It is important to determine how these hard power laws continue into the MeV range, because spectral features (lines, breaks, cut-offs) are unique fingerprints of non-thermal particle populations expected in those sources. GRIPS will probe accretion physics in the high-energy domain of stellar black holes, thus aid our understanding of the more-extreme circumstances encountered in accretion onto supermassive black holes.

2.7 Solar flares

Solar flare measurements will be a natural by-product of the continuous sky survey carried out by GRIPS as the Sun passes regularly through its field of view. The number of observed flares depends on the phase of the solar cycle during the GRIPS mission. Solar flare low-energy γ-ray spectra are characterized by a multitude of strong nuclear interaction lines, the annihilation line from β^+ radioactivity, and the neutron capture line at 2.2 MeV [13]. Lightcurves in characteristic (nuclear-line and continuum) energy bands and high statistics spectra provide the most direct visualization of how acceleration in highly dynamic cosmic situations works. In particular, it will be possible to determine the photospheric ^{3}He/^{4}He ratio [34] from the capture time history of energetic neutrons on protons seen in the emission of the 2.2 MeV deuterium formation line. The heavy-ion content of the interacting particles can also be derived from γ-ray spectroscopy and then compared to direct observations of solar energetic particles in interplanetary space, where large overabundances of ^{3}He ($\approx$100–1,000) and of low-FIP (first ionization potential) elements ($\approx$10–30) are found after impulsive-type flares. In this way the storage and escape of flare particles on the Sun can be studied. Gamma-rays in the MeV regime provide the means to directly study particle acceleration and matter interactions in these magnetised, non-thermal plasmas. Polarisation measurements are of great value for disentangling these dynamic processes.

Beyond this astrophysical reason, observing solar flares and 'space weather' are of great importance for our natural and technological environment. GRIPS would add an MeV-monitor to this program.

3 Mission profile

The GRIPS mission requires that a mass of 5.1 t be delivered into an equatorial, circular, low-Earth orbit (LEO) with an altitude of 500 km. The primary launcher requirements are determined by the low inclination LEO orbit and by the payload mass. The Soyuz Fregat 2B has a capacity of 5.3 t and is the only viable launch option in the Call. The GRIPS mission comprises two satellites containing the science instruments (Fig. 9): Gamma-Ray Monitor and the X-ray/Infrared telescopes respectively. These can readily be accommodated within the fairing specifications with a diameter of 3.8 m and a height of 7.7 m.

The orbit was selected to fulfill the following requirements in an optimized way: (i) low background, (ii) high science data fraction per orbit, (iii) high downlink rate for data transmission and good longitudinal coverage of the orbit by ground stations, (iv) high probability of the mission to remain at the chosen orbit for a mission life-time of $\approx$10 years. The requirement for a low background means low inclination, preferably 0° to avoid the radiation belts and the South Atlantic Anomaly. It is now well established that the background in hard X-ray and γ-ray instruments in a LEO can be a factor of 100 lower than in a Highly Eccentric Orbit, such as that of INTEGRAL.

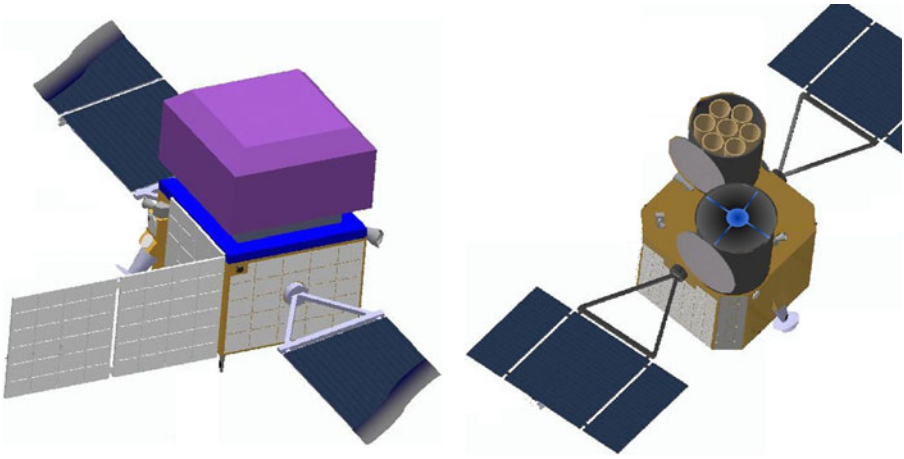

Fig. 9 GRIPS configuration in the two-satellite option, where the GRM is on one satellite (*left*), and XRM and IRT on the other (*right*). The GRM satellite would just do the zenith scanning all-sky survey, while XRM/IRT would re-point with the whole (second) satellite to GRBs, similar to *Swift*

Both satellites of GRIPS (with an inter-satellite distance of 500–2,000 km) should be 3-axis stabilized with closed loop attitude control, following the tradition of many recent astronomical space missions, and presenting no new problems in the control of the dynamics of the spacecrafts. GRIPS will have, however, three distinct features:

1. GRIPS/GRM will do zenith-pointing all the time.
2. For each localised GRB, GRIPS/XRM&IRT should be alerted via inter-satellite link and autonomously slew with the co-aligned X-ray and Infrared telescopes towards the GRB location, similar to Swift [17]. With ≈2 GRBs/day, a large fraction of the GRIPS/XRM&IRT satellite operation will be to follow-up GRBs. The envisaged strategy is to perform 3–5 pointings of 10–20 min duration per satellite orbit.
3. After the first ∼100 s X-ray observation the X-ray afterglow position will be determined with an accuracy of $<45''$, and another satellite slew commanded to place the afterglow in the IRT FOV. Despite the large X-ray FOV we expect no confusion of the afterglow with persistent X-ray sources for two reasons: (i) based on the X-ray afterglow intensity distribution at 30 min after the burst, 92% of all known X-ray sources are fainter than the faintest GRB afterglow, resulting in a chance coincidence of 10% to have one unrelated X-ray source in the total 7 square-degree FOV which is brighter than the faintest X-ray afterglow. (ii) From the ∼3 yr *eROSITA* survey after 2014 there will be a complete catalog of all faint X-ray sources (modulo variability) taken with exactly the same telescope/detector characteristics.

Highest scientific quality will be reached if all detected photons of GRM can be telemetered to Earth with all their interaction parameters. In GRM we expect about 68 000 cts/s, thus about 1.5 Mbps. The XRM produces about 110 cts/s, or 10.6 kbps, and the IRT about 1.2 Mbps. Since this has to be transmitted to ground in about 8 min passes out of 96 min orbital period, we require a downlink rate of 35 Mbps.

4 Proposed model payload

GRIPS will carry three major telescopes: the Gamma-Ray Monitor (GRM), the X-Ray Monitor (XRM) and the Infrared Telescope (IRT). The **GRM** is a combined Compton scattering and Pair creation telescope sensitive in the energy range 0.2–80 MeV. It will follow the successful concepts of imaging high-energy photons used in *COMPTEL* (0.7–30 MeV) and *EGRET* (>30 MeV) but combines them into one instrument. New detector technology and a design that is highly focused on the rejection of instrumental background will provide greatly improved capabilities. Over an extended energy range the sensitivity will be improved by at least an order of magnitude with respect to previous missions. In combination with improved sensitivity, the large field of view (FOV), better angular and spectral resolution of GRM will allow the scientific goals outlined in Section 2 to be accomplished (Table 1). The **XRM** is based on the mature concept and components of the *eROSITA* X-ray telescope, which is scheduled for a space mission on the Russian platform *Spektrum-XG* in 2013. The **IRT** is based on the telescope as proposed for the *EUCLID* mission. It uses the same main mirror and telescope structure (most importantly distance between M1 and M2). Instead of the suite of *EUCLID* instrumentation, just one instrument is foreseen: a 7-channel imager to determine photometric redshifts of GRB afterglows in the range $7 < z < 35$.

4.1 Gamma-ray monitor

Two physical processes dominate the interaction of photons with matter in the γ-ray energy band from 200 keV to ∼80 MeV: Compton scattering at low energies, and electron-positron pair production at high energies, with the crossover at ∼8 MeV for most detector materials. In both cases the primary interaction produces long-range secondaries whose directions and energies must be determined to reconstruct the incident photon properties.

Table 1 Scientific requirement vs. payload property

Large number of GRBs	Large FOV γ-ray detector
Detect spectral lines	3% spectral resolution; high continuum sensitivity
Detect polarisation	Record Compton events w. large scatter angle
Onboard localisation	Computing resource
Arcmin localisaton	X-ray telescope
Rapidly recognize high-z	IR telescope

4.1.1 Conceptual design and key characteristics

The GRM will employ two separate detectors as was the case for previous Compton and pair creation telescopes. The first detector is a tracker (D1), in which the initial Compton scattering or pair conversion takes place, and the other a calorimeter (D2), which absorbs and measures the energy of the secondaries (Table 2). In the case of Compton interactions, the incident photon scatters off an electron in the tracker. The interaction position and the energy imparted to the electron are measured. The scattered photon interaction point and energy are recorded in the calorimeter. From the positions and energies of the two interactions the incident photon angle is computed from the Compton equation. The primary-photon incident direction is then constrained to an event circle on the sky. For incident energies above about 2 MeV the recoil electron usually receives enough energy to penetrate several layers, allowing it to be tracked. This further constrains the incident direction of the photon to a short arc on the event circle. GRM will determine GRB locations to better than 1° (radius, 3σ).

The differential Klein–Nishina cross-section for Compton scattering contains a strong dependence on the polarisation of the incident γ-ray photon. Scattered photons are emitted preferentially perpendicular to the direction of the electric field vector of the incoming photon. The strongest azimuthal modulation in the distribution of scattered photons will be for the lowest γ-ray

Table 2 Gamma-ray monitor key characteristics

Detectors:		Mass + margin (kg)
D1	Si DSSD	50 + 2.5
	Structure	20 + 4
D2	$LaBr_3$	500 + 25
	Structure	240 + 48
ACS	Plastic	130 + 6.5
	Structure	40 + 8
Electronics		420 + 84
Total GRM		1,578
Channels	D1	196,608
	D2	104,960
	ACS	8
Total		301,576
Geometric area	D1/D2	6,400/10,752 cm^2
Energy resolution @ 662 keV (1σ)	D1/D2	1.0 keV/12.3 keV
Trigger thresholds @ 662 keV	D1/D2	10 keV/20 keV
Noise thresholds @ 662 keV	D1/D2	5 keV/10 keV
Background trigger rate (>5 keV)	LEO, $i = 0°$	68,000 cts/s
ARM (FWHM)	at 1 MeV	1.8 deg
Localisation	onboard	~0.5 deg
Cont. sensitivity @ 1 MeV ($\Delta E/E \approx 1$)	10^6 s, scan	3×10^{-5} ph/cm^2/s

energies and scattering angles of 60–90°. This makes a Compton telescope with a calorimeter covering a large solid angle a unique polarimeter.

In the case of pair production, the incident photon converts into an electron-positron pair in the tracker. These two particles are tracked and determine the incident photon direction. The total energy is measured through the deposits absorbed in the tracker and/or the calorimeter.

In addition to the 'telescope-mode' described above, the D2 detectors can also be read out in the so-called 'spectroscopy-mode', i.e. recording interactions that deposit energy only in the calorimeter. Using the side walls and the bottom of D2 as separate units a coarse localisation and high-quality spectra of GRB events can be obtained. This mode of operation follows the examples of BATSE on CGRO, the ACS in INTEGRAL and the GBM on Fermi.

4.1.2 GRM design, simulations and electronics

The design of a new high-energy γ-ray telescope must be based on numerical simulations as well as experimental detector developments. The baseline design and input to the Monte-Carlo simulations of the GRM is shown in Fig. 10. The top part shows the detector head with the central stack of double-sided Si-strip detectors (tracker D1) surrounded by the pixelated calorimeter (D2) and an anticoincidence system (ACS) made of plastic scintillator. The simulations were carried out with the tools of the MEGALIB software suite [47, 48], which, in addition to allowing modelling of the instrument functions, also generates realistic background environments and traces their impact on the telescope for the chosen orbit. Below the γ-ray detector are the GRM

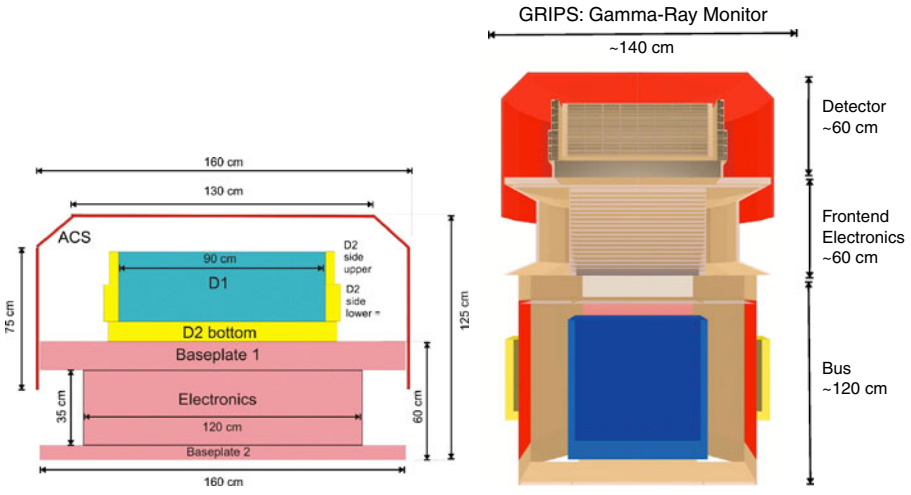

Fig. 10 *Left* Geometry and size of the detector module used for the simulations. *Right* Expected size and assembly of the Gamma-Ray Monitor and related electronics (*top*) on a generic satellite bus (*bottom*)

electronics and a generic spacecraft bus. In the simulations the bus of the Advanced Compton Telescope study was used [8].

The D1 detector consists of 64 layers each containing a mosaic of 8×8 double-sided Si strip detectors of area $10 \times 10\,\mathrm{cm}^2$, each of those having 96 strips per side. The layers are spaced at a distance of 5 mm. The D2 calorimeter is made of $LaBr_3$ prisms ($5 \times 5\,\mathrm{mm}^2$ cross-section; 35 photoelectrons/keV measured in the lab) which are read out with Si Drift Diode (SDD) photodetectors. The upper half of the D2 side walls feature scintillators of 2 cm length and the lower half has 4 cm thick walls. The side wall crystals are read out by one SDD each. The bottom calorimeter is 8 cm thick and is read out on both ends of the crystals to achieve a depth resolution of the energy deposits.

The whole detector is surrounded by a plastic scintillator counter that acts as an ACS against charged particles. Read out of the scintillation light, which is collected with embedded wavelength-shifting fibers to ensure the ACS uniformity, will be done with Si APD detectors.

Most of the structural material that holds the detector elements will be fabricated with carbon-fiber compounds rather than aluminum in order to reduce the background of activation radioactivity produced by cosmic-rays. The parameters and properties of the detector subsystems that were used in the simulations are listed in Table 2.

The layout of the GRM electronics is unchanged relative to our CV2007 proposal, and the interested reader is referred to [19].

4.1.3 Performance

GRIPS GRM features marked improvements when compared to the previous generation of Compton and pair creation instruments. The tracking volume (D1) embedded in the well-type calorimeter (D2) affords a large solid angle to detect the scattered components, which leads to a much wider FOV than *COMPTEL*, and moreover to a good polarimetric response. Low-energy pair particles are imaged in the tracker with much less scattering because, in contrast to the *EGRET* and *Fermi-LAT* chambers with their metal conversion plates, the GRM has very thin and fully active tracking detectors.

These performance enhancements can only be quantified numerically taking into account the interaction, detection, and reconstruction processes. Therefore, the performance of the GRM in an equatorial low-Earth orbit was extensively simulated with the MGGPOD suite and analyzed with the MEGAlib package (see [48] for an earlier version). MEGAlib contains a geometry and detector description tool that was used to set up the detailed modelling of the GRM with its detector types and characteristics. The geometry file is then used by the MGGPOD simulation tool to generate artificial events. The event reconstruction algorithms for the various interactions are implemented in different approaches (χ^2 and Bayesian). The high level data analysis tools allow response matrix calculation, image reconstruction (list-mode likelihood algorithm), detector resolution and sensitivity determination, spectra retrieval, polarisation modulation determination etc. Based on many

Table 3 Continuum point-source sensitivity of the Gamma-ray monitor after 10^6 s effective exposure; $\Delta E/E \sim 1$ and comparison with previous instruments

E (MeV)	GRIPS		Other[a]
	On-axis pointing (ph/cm^2/s)	All-sky scan (average) (ph/cm^2/s)	On-axis pointing (ph/cm^2/s)
0.2	4.0×10^{-5}	1.3×10^{-4}	I: 1.4×10^{-4}
1.0	1.0×10^{-5}	2.9×10^{-5}	C: 4.0×10^{-4}
5.0	6.5×10^{-6}	2.8×10^{-5}	C: 8.0×10^{-5}
20	1.0×10^{-6}	4.9×10^{-6}	C: 1.0×10^{-5}
50	3.2×10^{-7}	1.0×10^{-6}	E: 7.8×10^{-7}
80	2.4×10^{-7}	7.9×10^{-7}	E: 2.5×10^{-7}

[a] *C* COMPTEL, *I* IBIS, *E* EGRET

billions of simulated events we have derived a good understanding of the properties of GRIPS. Fine-tuning the detector concept since the CV2007 proposal has led to a substantial reduction in read-out channels at identical sensitivity.

Continuum sensitivity GRIPS will achieve a major improvement in sensitivity over previous and presently active missions (Table 3), e.g. a factor 40 improvement over *COMPTEL* around 1–2 MeV, or a factor of >20 over IBIS above 300 keV. The FOV (Fig. 11) extends to large off-axis angles: in 'telescope-mode' up to ∼50° incidence angle for the 50% level, or all-sky in 'spectroscopy-mode'.

Line sensitivity The narrow-line point-source sensitivity of the GRM for three astrophysically important γ-ray lines is given in Table 4. For the standard operation mode, the all-sky scan, the resulting sensitivity is slightly worse than in pointing mode since the exposure is distributed over most of the sky and not concentrated into a small FOV like for INTEGRAL. This reduction is, however, offset by the large geometrical factor (effective area × solid angle),

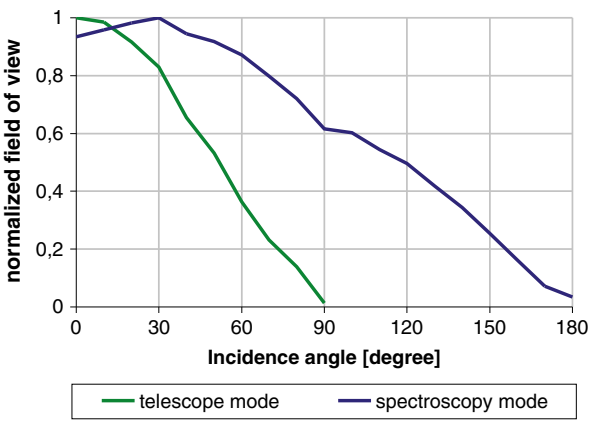

Fig. 11 Field of view of the Gamma-Ray monitor. In spectroscopy mode it is nearly 2π

Table 4 Narrow-line point-source sensitivity of the GRM after 10^6 s effective exposure

E (keV)	GRIPS		SPI
	On-axis pointing (ph/cm^2/s)	All-sky scan (average) (ph/cm^2/s)	On-axis pointing (ph/cm^2/s)
511	3.4×10^{-6}	1.5×10^{-5}	5.1×10^{-5}
1,157	2.4×10^{-6}	7.8×10^{-6}	3.0×10^{-5}
1,809	1.5×10^{-6}	4.1×10^{-6}	3.2×10^{-5}

the uniformity of the scan, and the permanent accumulation of exposure. As a consequence, after 5 years in orbit, GRIPS will achieve a factor 40 sensitivity improvement over *COMPTEL* (in 9 years) in e.g. the 1,809 keV line. A breakdown into the various factors is shown in Table 5. COMPTEL's capability to discriminate upward moving photons (using its time-of-flight measurement) and suppress neutron events (via its PSD selection) is matched by GRIPS capability to determine the direction of motion of the photon and suppress non-photon events using electron tracking and multiple Compton interactions (see [46]).

Polarisation Linearly polarised γ–rays preferentially Compton scatter perpendicular to the incident polarisation vector, resulting in an azimuthal scatter angle distribution (ASAD) which is modulated relative to the distribution for unpolarised photons. The sensitivity of an instrument to polarisation is given by the ratio of the amplitude of the ASAD and its average, which is called the modulation factor μ. The modulation is a function of incident photon energy, E, and the Compton scattering angle, θ, between the incident and scattered photon directions (see Fig. 12 or 13 for the MEGA prototype calibration).

GRIPS is a nearly perfect polarimeter (Fig. 14): The well-type geometry allows the detection of Compton events with large scattering angles which carry most of the polarisation information. The best polarisation sensitivity is achieved in the 200–400 keV range.

Maintaining the uniformity of response of the azimuthal detectors (mainly the side wall calorimeter units) is highly important to assess potential polarization signatures. There are at least three methods that will be employed:

Table 5 Break-down of GRIPS improvement relative to COMPTEL at 1.8 MeV

Parameter	COMPTEL	GRIPS	Improvement	Sensitivity improvement
Effective area (similar selection)	16 cm^2	195 cm^2	12.2	3.49
Observing time (pointing vs. scanning)	0.35	1	2.9	1.69
Energy resolution (1σ)	59 keV	17 keV	3.5	1.87
Angular resolution (FWHM)	3°.9	1°.5	2.6	1.61
Field-of-View (HWHM)	30°	45°	2.2	1.48
Background (orbit, passive material, tracker shielding)			3.0	1.73
Total				45.5

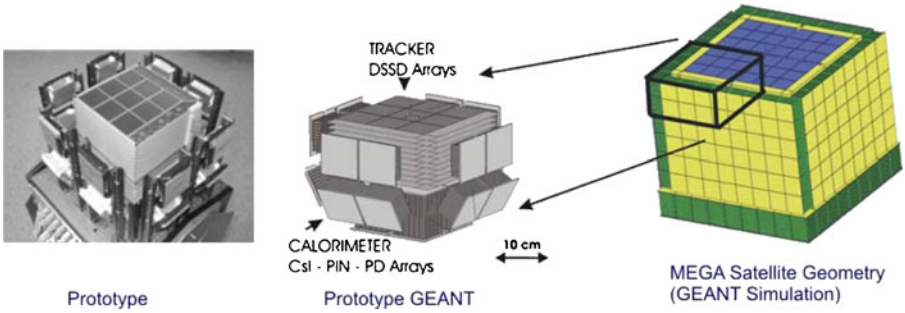

Fig. 12 The GEANT models for the MEGA satellite version (*right*), prototype (*middle*) and a photograph of the actual prototype detector (open to show the DSSD and CsI detectors). Note that for the proposed GRIPS concept, CsI is replaced by $LaBr_3$

(i) in pre-flight calibrations the uniformity will be calibrated with radioactive sources. During the mission the unavoidable background spectra due to local radioactivity will be monitored to calibrate the long-term stability of every detector cell. The necessary modes of data acquisition (i.e. single event triggers in D2) can be activated on demand, (ii) during the observation of astrophysical sources that are expected to be unpolarized (e.g. the ^{26}Al line) the azimuthal scattering distribution can be 'flat fielded', and (iii) the GRIPS platform flies with a zenith pointing attitude and therefore rotates with respect to the celestial sphere once per orbit around the normal to the orbital plane. A polarized source passing through the field of view will therefore be recorded in instrument coordinates with a turning polarization angle. This characteristic can be used to recognize and correct non-uniformities in the response of the D2 subsystem.

Gamma-ray bursts We have created model spectra with parameters for E_{peak}, high-energy power law slope β and peak flux, which cover their distribution as

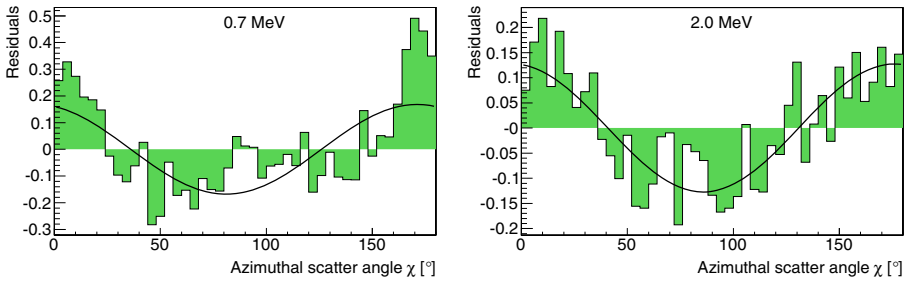

Fig. 13 Measured polarisation response of the MEGA prototype for two different energies. Within measurement errors and statistics, all values are in agreement with GEANT4 simulations: the polarisation angle of 90° is reproduced to 82% ± 24% (0.7 MeV) and 86% ± 11% (2.0 MeV), respectively. The measured modulation is 0.17 ± 0.04 and 0.13 ± 0.03 as compared to the simulated values 0.19 (at 0.7 MeV) and 0.14 (2.0 MeV) (from [46])

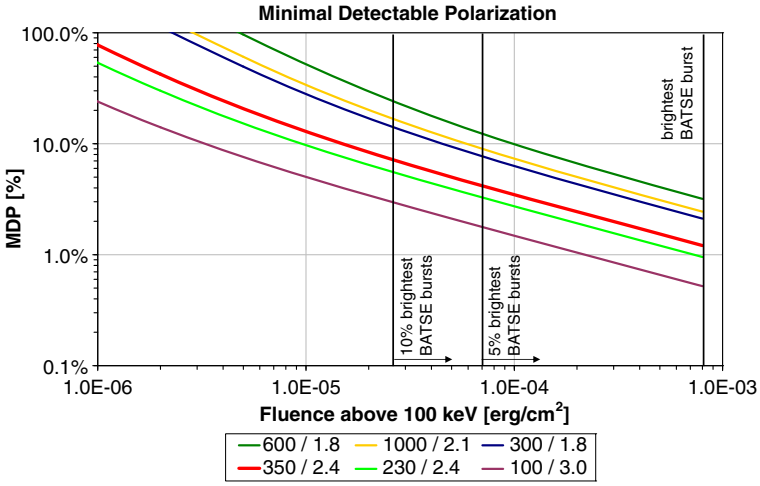

Fig. 14 Polarisation sensitivity of GRM. Various models of GRB spectra are shown which differ in their break energy and their high-energy power law slope; see legend for the parameter pair for each model. Note that at the bright end the minimal detectable polarisation changes much more slowly than the fluence

observed with BATSE (4th BATSE catalog; [33]). Note that the GBM/Fermi distribution of these parameters is, within statistics, identical to those of BATSE despite the wider energy range of GBM, thus indicating that the parameter space is complete. The faintest BATSE GRBs are clearly 'detected' by GRIPS with spectra extending from 100 keV up to 2 MeV and having more than 5 energy bins with 3σ each. From these simulations we estimate that GRIPS will be a factor of 3 more sensitive than BATSE below 1 MeV and detect about a factor of 2.5 more GRBs than BATSE. Folding in the smaller field of view of GRIPS compared to BATSE, we find that GRIPS will detect 665 GRBs/yr. For GRBs at an off-axis angle of $>70°$, only poor localisations, if any, will be possible, so we expect 440 GRBs/yr with good positions and XRM follow-up.

The present Swift samples of GRBs, both large biased samples as well as smaller but nearly complete samples [20], indicate a fraction of $5.5 \pm 2.8\%$ GRBs at $z > 5$. Using standard cosmology and star formation history description, this translates into a fraction of 1% of all GRBs located at $z > 10$, or 0.1% of all GRBs at $z > 20$. With 440 GRBs per year, and a nominal lifetime of 5 years (goal 10 years) we would expect 22 (goal 44) GRBs at $z > 10$, and 2 GRBs (goal 4) at $z > 20$. This includes a duty cycle of the instrument similar to that of BATSE and a detection rate of X-ray afterglows of 98%, as for Swift/XRT. Measurements with the IRT will ensure that high-z ($z > 7$) candidates are flagged immediately, and thus receive special attention in the optical/NIR identification and spectroscopic follow-up. The above numbers imply that (1) the detection frequency of GRBs at $z > 20$ is high enough to achieve at least one detection during the mission lifetime, and (2) that GRIPS

will clearly detect the cut-off in the z-distribution IF star formation starts at a certain redshift (below ∼25) throughout the Universe. Measuring this cut-off, or no cut-off up to $z \sim 25$, would in turn be a limit to the earliest time when stars formed.

Number of expected sources. Extrapolation from Swift/BAT (15–150 keV) Since this requires the assumption that the spectra do not cut off at some intermediate energy, we base our extrapolation on the 10% fraction of blazars (out of the total AGN population) for which there is no spectral break. We assume conservatively a photon index of −1.5 and using the logN-logS identified during the first three years of Swift/BAT [5], we find that GRIPS will detect, in a 1 year exposure, about 820 blazars in the 1–10 MeV band, among those 4 at $z > 8$.

Extrapolation from Fermi/LAT Fermi/LAT located 1451 sources during its first year survey (1FGL). About 700 objects are associated with extragalactic sources and include blazars, Seyfert and starburst galaxies. Among the identified galactic sources about 60 young pulsars and PWNe and 20 ms pulsars stand out, but many low galactic latitude sources are also associated with SNRs and a few high-mass X-ray binaries were detected. Detection or non-detection of all 1FGL sources in the adjacent lower energy range will be extremely important to understand their radiation processes. We estimate the detectability of the 1FGL sources in the 1–50 MeV range by extrapolating the power-law spectra measured by the LAT above 100 MeV, with the caveat that the spectrum could turn over (many EGRET-COMPTEL correlations showed spectral breaks in the 1–10 MeV range). We use not only the 1FGL spectral index (SI) but also the uncertainties, ie softer (S.I. + error S.I.) or harder (S.I. − error S.I.) spectral indices. For the 1–10 MeV range we find that between 860 and 1,200 1FGL sources are detectable (Table 6), and between 420 and 740 in the 10–50 MeV range.

Predictions from theory/modelling The number of new source types in the "discovery space" domain is more difficult to estimate. Based on theoretical predictions of emission properties (dominant energy band, fluxes) and

Table 6 Number of expected sources of various classes after 1 year and 5 years of GRIPS exposure

Type	1 year	5 years	New
GRBs	660	3,300	3,300
Blazars	820	2,000	400
Other AGN (100–300 keV)	250	300	0?
Pulsars/AXP	30	50	0?
Supernovae (Ia and cc)	2	20	20
Unidentified sources	170	230	60

The last column gives the number of completely new sources, not known before in any other wavelength. In addition, about 1,500 steady sources known in other wavelength bands will be detected in the MeV band for the first time

folded with the GRIPS sensitivity and the all-sky survey mode yields the following numbers: wind-collisions in high-mass binaries (200 keV): 30; superbubbles/star-forming regions (0.5–7 MeV): 20–200; microquasars/BH transients (200 keV/511 keV): 2/yr; supersoft sources (2.2 MeV): 10; flare stars (200 keV): 10/yr; galaxy clusters (4–7 MeV): 50.

4.1.4 Operation

The GRM instrument is highly pixelated and features about 3×10^5 fast measurement channels. Thus, the power (≈300 W), cooling (≈100 W) and data handling resources are large, but not challenging. According to our design, the electronics will be placed in a separate compartment from the detector units (see Fig. 10). Only a pre-amplifier and line driver will be integrated directly on the detectors, allowing the signals to be conducted to the remote (1–1.5 m distance) electronics. In this way the heat dissipation in the very densely packed detector unit will be minimised and the operating conditions of around 10° C can be established by passive thermal maintenance. The overall thermal layout, one of the major challenges of our CV2007 proposal [19], has been drastically mitigated by reducing the number of channels. We used a conservative 1mW/channel power consumption as compared to the already achieved ∼0.5 mW/channel consumption for the STARX32 ASIC [12], developed specifically for X- and γ-ray pixel detectors.

GRM will generally be operated in a continuous zenith pointed scanning mode. The field of view (diameter 160°) will cover most of the sky over the course of one orbit, similar to the all-sky survey performed by LAT on *Fermi*. Since the XRM/IRT are on a separate satellite, their frequent pointing changes have no impact on the GRM survey.

4.2 X-ray monitor

The main driver for the design of the X-ray monitor (XRM) is the positional accuracy of GRBs, so that their full error circle can be covered by the XRM. GRM will determine GRB positions to better than 1° (radius, 3σ) down to off-axis angles of 60°. We add a 50% margin, and require a field of view of the XRM of 3° diameter.

The second requirement is for sensitivity which should be at least a factor 3 larger than that of *Swift*'s XRT, since GRIPS will cover more distant GRBs, and thus likely fainter afterglows. Such sensitivity requirement (of order >300 cm^2) excludes coded mask systems, and even single-telescope Wolter-I optics are problematic.

4.2.1 Measurement technique, design and key characteristics

We therefore embark on a design consisting of multiple Wolter-I telescopes. The easiest and probably most cost-effective option is to adopt the *eROSITA* scheme of seven Wolter-I telescopes (Fig. 15), and adjust their orientation

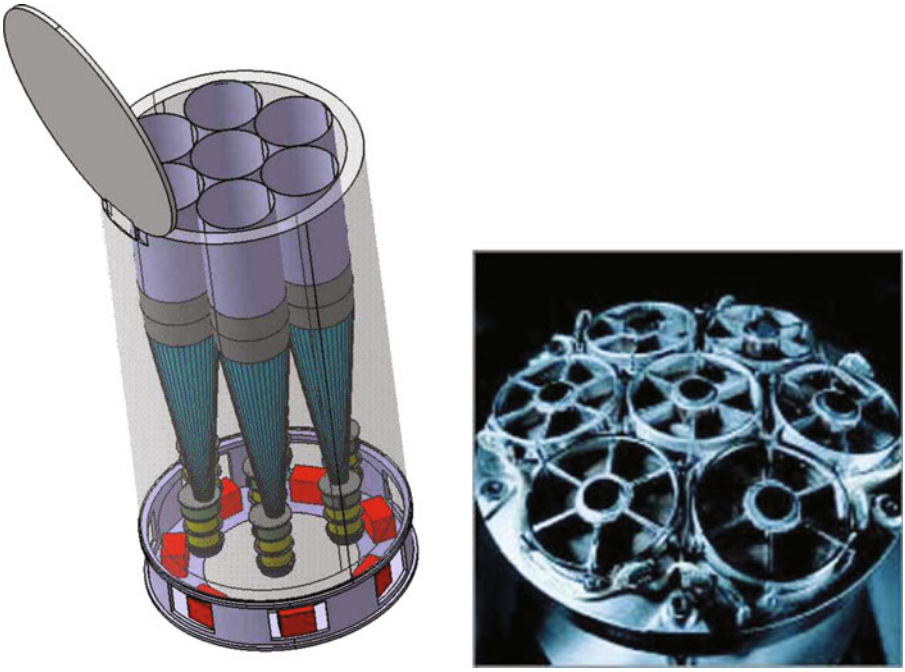

Fig. 15 Scetch of the 7-telescope configuration (*left*) and the prototype telescope array mounting (*right*) of eROSITA which will be adapted for the XRM of GRIPS

on the sky such that they fill the required FOV. *eROSITA* (for **e**xtended **RO**entgen **S**urvey with an **I**maging **T**elescope **A**rray) shall perform the first imaging sky survey in the medium X-ray range, i.e. between 0.2 and 12 keV, with a sensitivity of 9×10^{-15} erg cm^{-2} s^{-1} (0.2–2 keV) and 2×10^{-13} erg cm^{-2} s^{-1} (2–10 keV) [37]. This will allow the detection of about 3.2 million AGN, and ≈100.000 clusters of galaxies.

The satellite will be launched with a Soyus–Fregat rocket from Baikonur. The *eROSITA* instrument development is led by MPE Garching, and the main key characteristics are summarized in Table 7.

Table 7 Key characteristics of the XRM and detector (eROSITA Design Doc; MPE 2006)

Number of mirror modules	7
Degree of nesting	54
Focal length	1,600 mm
Largest mirror diameter	360 mm
Smallest mirror diameter	76 mm
Energy range	∼0.2–12 keV
Field-of-view	61′ ⊘
Angular resolution (HEW)	28″ (FOV-averaged)
Effective area (single telescope)	330 cm^2 at 1.5 keV/20 cm^2 at 8 keV
Mass per module	68 kg

4.2.2 Performance

We mention a number of improvements of the *eROSITA* detector over the *XMM*-Newton EPIC/PN detector: (i) lower noise and very homogeneous over detector pixels, (ii) smaller charge transfer losses, (iii) higher energy resolution, especially for low X-ray energies (<1 keV), (iv) smaller number of out-of-time events due to frame-store technique, (v) higher time resolution of 50 ms. As with the *XMM*-Newton EPIC/PN, the *eROSITA* detectors will share the high quantum efficiency (>90% over 0.2–12 keV band), the high radiation hardness against high energy protons including self-shielding against the low energy protons focused by the Wolter telescope. The effective area of the *eROSITA* telescope, even after placing all seven telescopes at different sky positions, well matches the GRIPS requirements (Fig. 16).

If a γ-ray burst is detected, the GRM satellite will autonomously issue a slew of the XRM/IRT satellite onto the target. To control the XRM/IRT pointing, two star-sensors will be mounted on each of the telescope structures. The autonomous pointing strategy has been shown on the *Swift* mission to be of very high scientific interest.

eROSITA is a fully funded project in collaboration with Russia, scheduled for launch in 2013. For a planned launch of the M mission in 2020–2022, instrument implementation will start around 2014/15, i.e. after completion and launch of *eROSITA*. Thus, not only will all technological problems be solved, but also all lessons learned during the development and assembly of *eROSITA* can be incorporated into the design of the XRM (Table 8).

4.3 Infrared telescope

The main driver for the design of the Infrared Telescope (IRT) is the goal to rapidly identify those GRBs which are at high redshift, so that particular

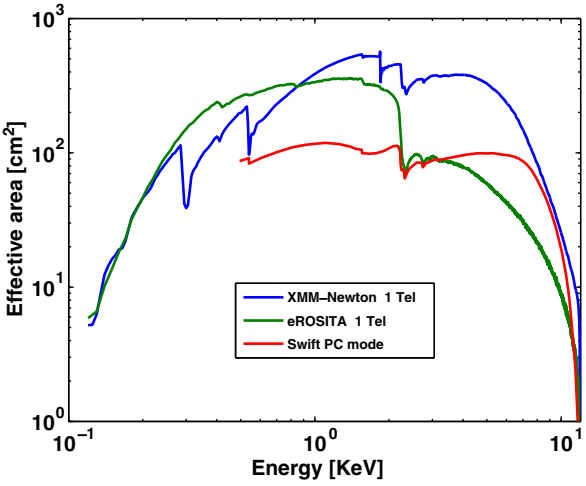

Fig. 16 Comparison of the effective area of the modified eROSITA system as proposed for the XRM (one telescope per sky position) with those of XMM and Swift/XRT

Table 8 XRM resources

Total eROSITA mass (incl. margin)	635 kg
Power eROSITA electronics	125 W
Power mirror/telescope heating	140 W
Telemetry events (average, 7 tel.)	7.0 kbit/s
Telemetry HK (average, 7 tel.)	3.6 kbit/s
On-board data storage (per day)	128 Mbyte

care can be devoted to their non-GRIPS follow-up observations. After the slew to a GRB, the XRT will provide a position with an accuracy between 15–50″ depending on the off-axis angle of the GRB in the XRT FOV. This uncertainty is too large for immediate (low-resolution) spectroscopy, so we resort to imaging.

4.3.1 Measurement technique, design and key characteristics

We propose simultaneous multi-band photometry in seven channels, zYJHKLM (Fig. 17) to determine photometric redshifts of GRBs (Fig. 3). Since GRB afterglow spectra are simple power laws, and at $z > 3$ Lyman-α is THE dominant spectral feature, relatively high accuracies can be reached even with broad-band filters (Fig. 3), as demonstrated in ground-based observations with GROND [28].

Since the *LM* band afterglow detections require a 1 m class telescope (see below), the most cost-effective way is a copy of the telescope as presently

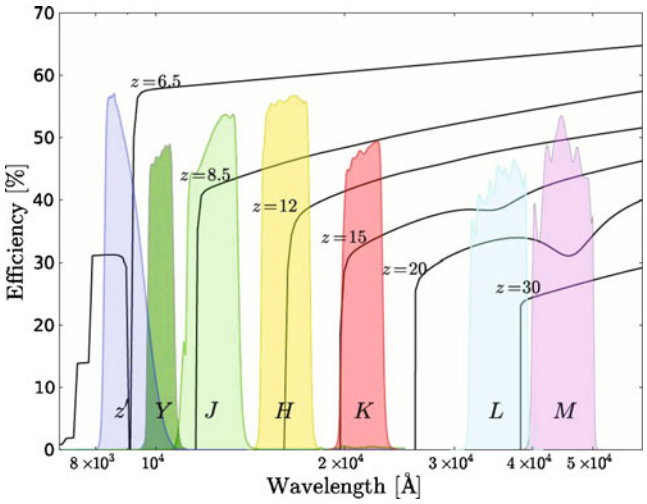

Fig. 17 Scetch of the proposed filter bands z'YJHKLM for the IRT. The efficiencies include best-effort estimates of all optical components, including the telescope, dichroics, filters and detector. Shown in *black lines* are template afterglow spectra, from redshifts $z = 6.5, 8.5, 12, 15, 20$ *to* 30 (*top left* to *bottom right*). These spectra also differ in their spectral index ($z = 6.5$ vs. all others) and rest-frame extinction (amount and reddening law; e.g. $z = 8.5$ and $z = 20$, the latter of which shows a redshifted 2,175 Å dust feature

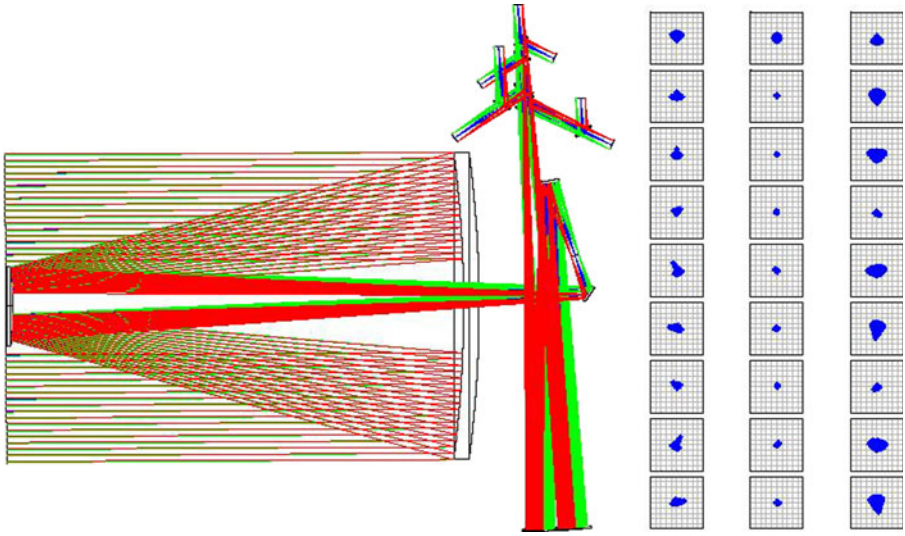

Fig. 18 *Left* Basic concept of the IRT with its seven photometric channels. M1 (diameter, curvature, but not conic constant) as well as the distance between M1 and M2 are identical to the EUCLID concept. M3 to M5 just serve as flat folding mirrors to minimize the size. *Right* Spot diagram of our ZEMAX design, for channels YJ (pass through one dichroic, *left*), z (only reflections, *center*), and M (pass through four dichroics, *right*). The *top row* is for the center of the FOV, and the other eight rows are for the sides and corners of the $10' \times 10'$ FOV. The *large boxes* are 18 μm on a side, corresponding to one H2RG pixel, and the small grid is 1.8 μm

proposed for the EUCLID mission, but with much reduced requirements for the tolerances in the alignment of the mirrors, in particular the PSF ellipticity, and long-term stability. We have replaced the EUCLID instrumentation with a system of dichroics which split the beam into the seven passbands (Fig. 18), very similar to the GROND concept [18]. Basic characteristics are given in Tables 9 and 10.

The baseline detector is a 2,048 × 2,048, 18 μm pixel, 2HRG detector from Teledyne Imaging Sensors. Depending on the channels, different cut-off wavelengths of 1, 2.5 and 5 μm will be chosen, respectively. The read-out, analog-to-digital conversion as well as first image processing is done by SIDECAR (System for Image Digitalization, Enhancement, Control and Retrieval) ASICs, also available from Teledyne. Control electronics and

Table 9 IRT key characteristics

Parameter	Value
Telescope	1.2 m Korsch
Filter	zYJHKLM (simultaneous)
FOV	$10' \times 10'$
Detectors	7 2K × 2K HAWAII
Plate Scale	$0''.3$/pixel
Sensitivity (5σ, 500 s exp)	24/23 mag AB (z-K/LM)

Table 10 IRT resources

Mass telescope (incl. margin)	130 kg
Mass instrument (optics+electronics)	150 kg
Power electronics	125 W
Power LM-band cooling	200 W
Raw data/day (2.5× compressed)	100 Gbit

post-processing/analysis CPU will be similar, but much simpler due to a substantial reduction in the number of moving parts (thus less control electronics, drivers, position sensors) than that presently designed for EUCLID.

4.3.2 Performance

Based on a complete sample of GRB afterglow measurements obtained with GROND since 2007 [20], in particular the afterglow brightness distribution in each of the g'r'i'z'JHK channels, we derive a minimum afterglow brightness of $M(\mathrm{AB}) \approx 22$ mag at 2 h after the GRB. Using standard parameters for the transmission of the optical components, read-out noise of the detector as well as zodiacal background light, a 1 m class telescope is needed to reach a 5σ detection with a 500-s exposure.

A ZEMAX design with the EUCLID baseline (a 3-mirror concept similar to DIVA/FAME/Gaia) and including all seven channels and three folding mirrors returns a perfect imaging quality with a Strehl ratio of 99% (right panel of Fig. 18) even for the worst channel (light passes through four dichroics). Estimates on the telescope have been adopted from the EUCLID Assessment Study Report (ESA/SRE-2009-2). Estimates on optics and detectors are based on GROND experience.

Similar to the GROND case [28], extensive Monte-Carlo simulations have been performed and demonstrate the accuracy with which the redshift can be determined (Fig. 3). The sample properties are chosen to be as close as possible to what is known about optical/NIR afterglows with respect to their spectral indices, neutral hydrogen column densities of their DLAs, and dust extinction. For the GROND case and $3 < z < 8.2$ range, these simulations are nicely confirmed by bursts which have also spectroscopic redshifts.

The XRM and IRT should be co-aligned such that the IRT FOV is centered in the FOV of the central X-ray telescope. They should have separate star-trackers to allow the boresight to be measured/tracked.

The IR detector temperatures need to be stable to within ± 0.1 K, thus each requiring a special control loop. The low operating temperatures (see critical issue below) and the frequent re-pointings of the XRM/IRT require special consideration of the thermal architecture.

An optical system with several dichroics in the converging beam (GROND) has been built and demonstrated to achieve $0\farcs4$ image quality [18]. Materials for similar systems up to 5μ are available, including radiation-hard versions.

4.4 Nice-to-have additions and option

There are two additional instruments which have been discussed in the preparation of this proposal, but are not proposed as default instrumentation due to lower priority.

(1) **Neutron-Monitor:** The neutron flux in a LEO varies with time, and induced γ-radiation in the telescope is a source of background. A small neutron detector would act as monitor of the general radiation field, and thus substantially help in fighting the background radiation.
(2) **Lobster X-ray monitor:** The Lobster camera principle is ideal for an all-sky monitor at soft X-rays with a spatial resolution in the few-arcmin range. It would allow detection of the prompt X-rays which are connected to the GRB prompt emission. A Lobster system, properly adapted to the GRIPS needs (ring-like FOV), would allow the localisation of (i) the $\sim$30% of GRBs for which the GRM will not be able to measure a position and (ii) those GRBs for which Earth or Sun constraints would prohibit slewing the XRT.

5 Summary

GRIPS would be an extraordinary tool to advance the study of the *nonthermal and violent Universe*.

The GRIPS mission would provide the data to answer key questions of high-energy astrophysics. Moreover, the all-sky survey with an expected number of more than 2,000 sources, many of them new, will at the same time serve a diversity of communities for the astronomical exploration of so-far unidentified X/γ-ray sources and of new phenomena. The delivery of triggers on bursting sources of high-energy emission will amplify the scientific impact of GRIPS across fields and communities. As the 2010 Decadal Survey Report of the US Academy of Science puts it, "Astronomy is still as much based on discovery as it is on predetermined measurements."

References

1. Abdo, A.A., et al.: Detection of the energetic pulsar PSR B1509-58 and its pulsar wind nebula in MSH 15-52 using the Fermi-large area telescope. Astrophys. J. **714**, 927 (2010)
2. Abdo, A.A., Ackermann, M., Ajello, M., et al.: The first catalog of active galactic nuclei detected by the Fermi large area telescope. Astrophys. J. **715**, 429 (2010)
3. Abdo, A.A., Ackermann, M., Ajello, M., et al.: Gamma-ray emission concurrent with the nova in the symbiotic binary V407 Cygni. Science **329**, 817 (2010)
4. Abdo, A.A., et al.: The first Fermi large area telescope catalog of gamma-ray pulsars. Astrophys. J. Suppl. **187**, 460 (2010)
5. Ajello, M., Greiner, J., et al.: BAT X-ray survey. I. Methodology and X-ray identification. Astrophys. J. **678**, 102 (2008)
6. Bai, X.-N., Spitkovsky, A.: Uncertainties of modeling gamma-ray pulsar light curves using vacuum dipole magnetic field. Astrophys. J. **715**, 1270 (2010)

7. Bai, X.-N., Spitkovsky, A.: Modeling of gamma-ray pulsar light curves using the force-free magnetic field. Astrophys. J. **715**, 1282 (2010)
8. Boggs, S.E.: Boggs: the advanced Compton telescope mission. New Astron. Rev. **50**, 604 (2006)
9. Böttcher, M., Reimer, A., Marscher, A.P.: Implications of the very high energy gamma-ray detection of the quasar 3C279. Astrophys. J. **703**, 1168 (2009)
10. Bouchet, L., Roques, J.P., Jourdain, E.: On the morphology of the electron-positron annihilation emission as seen by SPI/INTEGRAL. Astrophys. J. **720**, 1772 (2010)
11. Bromm, V., Loeb, A.: High-redshift gamma-ray bursts from population III progenitors. Astrophys. J. **642**, 382 (2006)
12. Caccia, S., Bertucci, G., Maiocchi, D., et al.: A mixed-signal spectroscopic-grade and high-functionality CMOS readout cell for semiconductor X-/γ-ray pixel detectors. IEEE Trans. Nucl. Sci. **55**, 2721 (2008)
13. Chupp, E.L., Ryan, J.M.: High energy neutron and pion-decay gamma-ray emissions from solar flares. Res. Astron. Astrophys. **9**, 11 (2009)
14. Cline, J.M., Frey, A.R., Chen, F.: Metastable dark matter mechanisms for INTEGRAL 511 keV γ rays and DAMA/CoGeNT events. Phys. Rev. **D83**, 083511 (2011)
15. de Jager, O.C., Slane, P.O., LaMassa, S.: Probing the radio to X-ray connection of the Vela X pulsar wind nebula with Fermi LAT and H.E.S.S. Astrophys. J. **689**, L125 (2008)
16. Gal-Yam, A., Mazzali, P., Ofek, E. O., et al.: Gal-Yam: supernova 2007bi as a pair-instability explosion. Nature **462**, 624 (2009)
17. Gehrels, N., Chincarini, G., Giommi, P., et al.: The swift gamma-ray burst mission. Astrophys. J. **611**, 1005 (2004)
18. Greiner, J., Bornemann, W., Clemens, C., et al.: GROND—a 7-channel imager. Publ. Astron. Soc. Pac. **120**, 405 (2008)
19. Greiner, J., Iyudin, A., Kanbach, G., et al.: Gamma-ray burst investigation via polarimetry and spectroscopy (GRIPS). Exp. Astron. **23**, 91 (2009)
20. Greiner, J., Krühler, T., Klose, S., et al.: The nature of 'dark' gamma-ray bursts. Astron. Astrophys. **526**, A30 (2010)
21. Hammer, N.J., Janka, H., Müller, E.: Three-dimensional simulations of mixing instabilities in supernova explosions. Astrophys. J. **714**, 1371 (2010)
22. Hooper, D., Ferrer, F., Boehm, C., et al.: Possible evidence for MeV dark matter in dwarf spheroidals. Phys. Rev. Lett. **93**, 1302 (2004)
23. Iyudin, A.F., Galkin, V.I., Dzhatdoev, T.A.: The possibility of observing resonance gamma-ray absorption in the spectra of active galactic nuclei. Astron. Rep. **53**, 102 (2009)
24. Kuiper, L., et al.: COMPTEL detection of pulsed gamma-ray emission from PSR B1509-58 up to at least 10 MeV. Astron. Astrophys. **351**, 119 (1999)
25. Kuiper, L., et al.: Hard X-ray timing and spectral characteristics of the energetic pulsar PSR J0205+6449 in supernova remnant 3C 58. An RXTE PCA/HEXTE and XMM-Newton view on the 0.5–250 keV band. Astron. Astrophys. **515**, A34 (2010)
26. Kuiper, L., Hermsen, W.: High-energy characteristics of the schizophrenic pulsar PSR J1846-025 in Kes 75. Multi-year RXTE and INTEGRAL observations crossing the magnetar-like outburst. Astron. Astrophys. **501**, 1031 (2009)
27. Kuiper, L., Hermsen, W., den Hartog, P.R., Collmar, W.: Discovery of luminous pulsed hard X-ray emission from anomalous X-ray pulsars 1RXS J1708-4009, 4U 0142+61, and 1E 2259+586 by INTEGRAL and RXTE. Astrophys. J. **645**, 556 (2006)
28. Krühler, T., Schady, P., Greiner, J., et al.: Photometric redshifts for gamma-ray burst afterglows from GROND and Swift/UVOT. Astron. Astrophys. **526**, A153 (2010)
29. Langer, N., Norman, C.A., de Koter, A., Vink, J.S., Cantiello, M., Yoon, S.-C.: Pair creation supernovae at low and high redshift. Astron. Astrophys. **475**, L19 (2007)
30. Limongi, M., Chieffi, A.: The Nucleosynthesis of ^{26}Al and ^{60}Fe in solar metallicity stars extending in mass from 11 to 120 Msolar: the hydrostatic and explosive contributions. Astrophys. J. **647**, 483 (2006)
31. Marion, G.H., Höflich, P., Vacca, W.D., Wheeler, J.C.: Near-infrared spectra of type Ia supernovae. Astrophys. J. **591**, 316 (2003)
32. Naoz, S., Bromberg, O.: Naoz & Bromberg: an observational limit on the earliest gamma-ray bursts. Mon. Not. R. Astron. Soc. **380**, 757 (2007)
33. Paciesas, W.S., Meegan, C.A., Pendleton, G.N., et al.: The fourth BATSE gamma-ray burst catalog. Astrophys. J. Suppl. **122**, 465 (1999)

34. Petrosian, V., Jiang, Y.W., Liu, S., Ho, G.C., Mason, G.M.: Relative distributions of fluences of ^{3}He and ^{4}He in solar energetic particles. Astrophys. J. **701**, 1 (2009)
35. Pilia, M., et al.: AGILE observations of the "Soft" gamma-ray pulsar PSR B1509-58. Astrophys. J. **723**, 707 (2010)
36. Prantzos, N., Boehm, C., Bykov, A.M., et al.: Prantzos: the 511 keV emission from positron annihilation in the galaxy. Rev. Mod. Phys. arXiv:1009.4620 (2011, in press)
37. Predehl, P., Andritschke, R., Böhringer, H., et al.: eROSITA on SRG. SPIE **7732E**, 23 (2010)
38. Ramaty, R.: Interstellar gamma-ray lines from low energy cosmic ray interactions. Astron. Astrophys. Suppl. **120**, 373 (1996)
39. Romani, R.W., Watters, K.P.: Constraining pulsar magnetosphere geometry with γ-ray light curves. Astrophys. J. **714**, 810 (2010)
40. Salvaterra, R., Della Valle, M., Campana, S., et al.: GRB090423 at a redshift of z∼8.1. Nature **461**, 1258 (2009)
41. Sim, S.A., Mazzali, P.A.: On the γ-ray emission of type Ia supernovae. Mon. Not. R. Astron. Soc. **385**, 1681 (2008)
42. Summa, A., Elsässer, D., Mannheim, K.: Nuclear de-excitation line spectrum of Cassiopeia A. Astron. Astrophys. **533**, A13 (2011)
43. Tanvir, N.R., Fox, D.B., Levan, A.J., et al.: A γ-ray burst at a redshift of z∼8.2. Nature **461**, 1254 (2009)
44. Tibolla, O., Mannheim, K., Paravac, A., Greiner, J., Kanbach, G.: GRIPS and its strong connections to the GeV and TeV bands. In: Proc. of "Gamma-ray Astrophysics in the Multi-messenger Context". Il Nuovo Cim. C **034**(3), 41 (2011)
45. Watters, K.P., Romani, R.W., Weltevrede, P., Johnston, S.: An atlas for interpreting γ-ray pulsar light curves. Astrophys. J. **695**, 1289 (2009)
46. Zoglauer, A.: First light for the next generation of Compton and Pair telescopes. PhD thesis, TU Munich (2006)
47. Zoglauer, A., Andritschke, R., Schopper, F.: MEGAlib the medium energy gamma-ray astronomy library. New Astron. Rev. **50**(7–8), 629 (2006)
48. Zoglauer, A., Andritschke, R., Boggs, S., et al.: MEGAlib: simulation and data analysis for low-to-medium-energy gamma-ray telescopes. SPIE **7011E**, 101 (2008)